NASA Contractor Report 159305

NASA-CR-159305
19800019808

DRAG REDUCTION EFFECTS IN TURBULENT BOUNDARY LAYERS OVER WAVY WALLS

R. Balasubramanian and Steven A. Orszag

CAMBRIDGE HYDRODYNAMICS, INC.
CAMBRIDGE, MASSACHUSETTS 02139

CONTRACT NAS1-15754

AUGUST 1980

NASA
National Aeronautics and Space Administration

Langley Research Center
Hampton, Virginia 23665

1. Report No.	2. Government Accession No.	3. Recipient's Catalog No.
NASA CR-159305		

4. Title and Subtitle	5. Report Date
DRAG REDUCTION EFFECTS IN TURBULENT BOUNDARY LAYERS OVER WAVY WALLS	August 1980
	6. Performing Organization Code

7. Author(s)	8. Performing Organization Report No.
R. Balasubramanian and Steven A. Orszag	CHI Report No. 41
	10. Work Unit No.

9. Performing Organization Name and Address	11. Contract or Grant No.
Cambridge Hydrodynamics, Inc. P.O. Box 249, M.I.T. Station Cambridge, Massachusetts 02139	NAS1-15754
	13. Type of Report and Period Covered

12. Sponsoring Agency Name and Address	
National Aeronautics and Space Administration Washington, D.C. 20546	Final
	14. Sponsoring Agency Code

15. Supplementary Notes

Contract Monitor: A.M. Cary, Jr., NASA Langley Research Center

16. Abstract

Two dimensional incompressible flow over wavy surfaces are analyzed numerically by spectral methods. Algorithms for (i) periodic flows (Fourier modes in the periodic flow direction and Chebycheff modes in the normal direction) and (ii) inflow-outflow boundary conditions (Chebycheff modes used in both directions) are described. Results obtained using both codes are reported for laminar flows. Comparisons with known theoretical and experimental results are made.

17. Key Words (Suggested by Author(s))	18. Distribution Statement
Drag reduction Spectral methods Incompressible flows	Unclassified - Unlimited

19. Security Classif. (of this report)	20. Security Classif. (of this page)	21. No. of Pages	22. Price*
Unclassified	Unclassified	42	

N-305

For sale by the National Technical Information Service, Springfield, Virginia 22161

N80-28309#

NOMENCLATURE

a	amplitude of the wavy surface
a_n	Fourier component of amplitude
A	Fourier-Tchebycheff expansion coefficient
C_p	coefficient of pressure
D	domain of analysis
f	right-hand side of Poisson equation (See Eq. 20)
F'	Jacobian of transformation
F_k	X-decomposition of function f (See Eq. 23)
$\hat{F}$	Fourier transformed variable
g	transformation coefficient
i	mode number
k	wave number
L	length scale used in squeezing transformation
m	mode number
M_c	mode cut-off number
n_N	Tchebycheff mode number convective terms (See Eq. 11)
N_c	Tchebycheff cut-off mode number
p	pressure
Pmin	minimum pressure
Pmax	maximum pressure
$\hat{p}$	Fourier transform of pressure
p_∞	free stream pressure
R	region of analysis
Re_X	Reynolds number based on length X
t	time

u	velocity vector
V	expansion function
x	distance in the flow direction
X	distance in transformed plane
y	distance in the normal direction
Y	distance in the transformed plane
δ	boundary layer thickness
η	coordinate in conformal mapped system
ϕ	phase angle
κ	eigenvalue
λ	Eigenvalue
ν	viscosity
σ	parameter in viscous stabilization
τ	stress tensor
ζ	coordinate in conformally mapped system

Superscripts:

$\sim$	explicit convective updated variable (See Eq. 10)
$\approx$	implicit values afterconvective update
$\hat{}$	pressure updated value
$-$	viscous update (explicit) See Eq. (25)
$=$	viscous stabilized values See Eq. (26)

INTRODUCTION

There is considerable experimental evidence (1, 2) that turbulent flow over wavy surfaces reduces skin friction drag sizeably. However, a favorable net drag reduction over wavy surfaces have not yet been reported mainly because of a pressure drag contribution in all of these experiments. In order to design wavy surfaces which have large skin friction drag reductions and insignificant pressure drag contribution, wave geometries of considerable complexities may need to be considered. The present investigation under NASA Contract NAS 1-15754, was motivated largely from these considerations and as an attempt to understand the underlying mechanism governing the details of flow changes over wavy surfaces through numerical simulation.

Work on flows in wavy geometries began with the classical Kelvin-Helmholtz analysis of linearised inviscid flows [3]. For a wall displacement of the form $y = a\cos(kx + \Phi)$ [where the assumption $ka << 1$ has to be made for the linearisation to hold] the Kelvin-Helmhotz theory predicts a pressure distribution at the wall of the form

$$p = p_\infty + \rho U_\infty^2 \, ka \cos(kx + \pi + \Phi) \qquad (1)$$

thus the pressure coefficient $Cp = \dfrac{p - p_\infty}{\frac{1}{2}\rho U_\infty^2}$ is $2ka$ at the wall.

The inviscid predictions overpredict the magnitude of the pressure distributions and have incorrect phase relations between

the pressure and the wall, for real flows. In order to improve the prediction techniques Miles[4] extended the inviscid theory to account for shear in the mean flow. Miles' theory improves the prediction of pressure coefficient; however, due to the inviscid nature of the analysis, the pressure distribution is still 180° out of phase with the wall. Benjamin[5] analysed high Reynolds number laminar flows over wavy walls including the effect of shear through asymptotic theory ($Ka \ll 1$). The pressure distribution at the wall, as predicted by his theory, has the correct phase and magnitude (for small amplitude waves in fairly high Reynolds number laminar flows).

There have been a large number of investigations of turbulent flow over gentle waves. A majority of these investigations consider that the wall perturbation (i.e. waviness) does not modify the turbulent process as such. Davis[6] has postulated that perturbation turbulent stresses be also included in analysing the problem. Zilker et al[7] have incorporated effects of self-generated pressure gradients in the length-scale models. Recently Markatos[8] has attempted the solution of wavy wall turbulent flow through a two equation turbulence model by finite difference techniques. While Markatos' numerical results are at best first order accurate in space, they go a long way towards providing understanding of the nature of flow over wavy walls.

The present work extends previous investigations in several ways. The full time-dependant two dimensional Navier Stokes equations are solved using spectral methods (to achieve high spatial

accuracy) and higher order time splitting methods together with conformal mapping methods to allow simulation of flow over steep waves ($ka \sim 0(1)$) Two basic computer codes have been developed under the present contract. The two specific codes described in this report are:

1) Code 1 - Periodic inflow-outflow conditions are used in the lateral direction for walls with spatial regularity. A spectral Tchebycheff-Fourier mode expansion is used (spectral Tchebycheff--in the normal direction of the flow, and Fourier--spectral in the direction of periodicity) to obtain infinite order accuracy in space. A second order accurate time scheme (Adams-Bashforth with Richardson extrapolation) is adopted in this code to obtain accurate time transients.

2) Code 2 - This computer code uses prescribed inflow-outflow conditions; a two dimensional Tchebycheff expansion scheme is used to guarantee high spectral accuracy. Again, second order time accuracies are obtained using Richardson extrapolation schemes.

In Section II the methods of solution adopted for the two codes are described. Results for laminar flows at various Reynolds numbers are presented in Section III. In Section IV, results for nonsymmetric waves are described. Finally, in Section V application of these codes to other flow problems and directions of future work are delineated.

II. METHODS OF SOLUTION

The two dimensional Navier Stokes equations are

$$\frac{\partial u}{\partial t} + u.\ \nabla u = -\nabla p + \nabla.\vec{\tau} \tag{1}$$

$$\nabla.u = 0 \tag{2}$$

where the stress tensor $\vec{\tau}$ may include both laminar stresses and turbulent stresses.

II. A METHOD OF SOLUTION FOR CODE I

For Code I the domain of analysis and the boundary conditions appropriate are

$$D:\ 0 < x < 2\pi \quad ,\quad f(x,t) \leq y \leq \infty \tag{3}$$

above the wall, $y = f(x,t)$

and

$$\begin{aligned} u(x,y,t) &= u(x+2\pi, y, t) \\ p(x,y,t) &= p(x+2\pi,y,t) \\ \vec{\tau}(x,y,t) &= \vec{\tau}(x+2\pi,y,t) \end{aligned} \tag{4}$$

The test results reported (using Code I) in this report are for the case where the wall is stationary, i.e.

$$f(x,t) = \sum_{n=1}^{m_c} a_n \cos(k_n x + \phi_n) \tag{5}$$

where m_c is the cut off mode number in the summation. A conformal mapping technique[9] is used to transform the domain (3) into the

region.

$$0 \leq \zeta \leq 2\pi, \quad 0 \leq \eta \leq \infty \tag{6}$$

When the slope of the wall $|ka| \leq 1$ the conformal mapping coefficients are accurately generated in only N log N operations where N is the resolution along $x(\zeta)$. Thus time-dependant geometries can be very efficiently handled through this mapping technique. A further stretching (non-conformal) transformation of η is carried out in order to implement the spectral method so that the domain (6) maps into the finite region,

$$R: \quad 0 \leq X \leq 2\pi, \; -1 \leq Y \leq +1 \tag{7}$$

by the transformation

$$X = \zeta, \quad Y = \frac{2\eta}{\eta+L} - 1$$

or

$$X = \zeta, \quad Y = 1 - 2\, e^{-\eta/L} \tag{8}$$

where L is some suitable mapping scale.

A plot of the mapped grid used in the computation is shown in Fig. 1. The wall is a sine wave ($m_c = 1, \phi_n = \pi$). The wall slope ka = 0.1963. Only a portion of the computational grid is shown in Fig. 1 (so as to keep x, y scales in plotting nearly equal). The vertical lines in Fig. 1 are lines of constant ζ, and the horizontal lines are lines of constant ($\eta : Y$) The orthonormality of the grid lines is quite apparent from the figure. Equations (1)--(2) are solved numerically by a fractional step

procedure. The procedure adopted is the spectral collocation technique. In this method, all dependant variables are expanded in Fourier Tchebycheff series as

$$F(X,Y,t) = \sum_{n=0}^{N} \sum_{|m| < m_c} A(n,m,t) e^{imX} T_n(Y) \qquad (9)$$

where $T_n(Y) = \cos(n \cos^{-1} Y)$ is the Tchebycheff polynomial of degree n. The fractional steps used in this procedure are:

(i) Convective update

(a) Explicit step

An intermediate field is found such that

$$\tilde{u} = u_n(x,y,t) + \frac{3}{2} \Delta t\, N(x,y,t_n) \frac{-\Delta t}{2} N(x,y,t_{n-1}) \qquad (10)$$

where

$$N(x,y,t) = - (u - U_m(Y)).\nabla u \qquad (11)$$

Um in Eq (11) is a mean profile (of the dominant velocity component in X direction)

(b) Implicit convective step

$$\tilde{\tilde{u}} + \Delta t\, Um \cdot \nabla \tilde{\tilde{u}} = \tilde{u} \qquad (12)$$

The application of the implicit step releases time step restrictions of Courant-Friedrichs-Lewy type $(\Delta t \leq \frac{\Delta x}{u})$

(ii) Pressure update

$$\hat{u} = \tilde{\tilde{u}} - \nabla p \tag{13}$$

$$\nabla \cdot \hat{u} = 0 \tag{14}$$

with the boundary conditions

$$n \cdot \hat{u} = 0 \quad (\text{at } \eta = 0) \tag{15}$$

from (13),

$$\nabla^2 p = \nabla \cdot \tilde{\tilde{u}} \tag{16}$$

with $\frac{\partial p}{\partial \eta} = 0$ (for a stationary wall) (17)

The boundary conditions in ζ directions are already satisfied by the assumption of periodicity of the flow.

(iib) Fast poisson solver

Solution of (16) with (17) is implemented through a fast Poisson algorithym. The conformality of mapping between (x, y) to (ζ, η) provides

$$\nabla^2 p = |F'|^2 \left(\frac{\partial^2 p}{\partial \zeta^2} + \frac{\partial^2 p}{\partial \eta^2}\right) \tag{18}$$

The right hand side of (18) can be written as

$$\nabla^2 p = (F')^2 \left(\frac{\partial^2 p}{\partial X^2} + g(Y) \frac{\partial}{\partial Y}\left(g(Y)\frac{\partial p}{\partial Y}\right)\right) \tag{19}$$

where $g(Y) = \frac{\partial Y}{\partial \eta}$

Equation (16), therefore, modifies to

$$\frac{\partial^2 p}{\partial X^2} + g(Y)\frac{\partial}{\partial Y}\left(g(Y)\frac{\partial p}{\partial Y}\right) = f(X,Y) \tag{20}$$

In order to solve Eq (20) efficiently, we introduce the eigenvalue problem,

$$g(Y)\frac{\partial}{\partial Y}\left(g(Y)\frac{\partial u}{\partial Y}\right) = \lambda u \tag{21}$$

subject to the homogeneous boundary conditions,

$$\frac{\partial u}{\partial Y} = 0 \qquad @ \quad Y = -1 \tag{22}$$

The eigen values and the eigenfunctions associated with this problem (21) are found in a pre-processing step. The function u(X, Y) can therefore be expanded as,

$$u(X,Y) = \sum_k V_k(X)\, u_k(Y) \tag{23}$$

and similarly

$$f(X,Y) = \sum_k F_k(X)\, U_k(Y)$$

Thus Eq (20) can be written as

$$\sum_{|i|=0} \sum_{k=0} ((i-1)^2 + \lambda_k)\, \hat{p} = \hat{F} \tag{24}$$

where the tilda stands for fourier transformed variables. Solution of the poisson equation is thus accomplished through further matrix operations of Eq (24).

(iii) Viscous update

$$\bar{u} = \hat{u} + \Delta t \quad \nabla \cdot \vec{\tau}_n \tag{25}$$

with the boundary condition

$$\bar{u} = 0 \qquad @ \qquad \eta = 0$$

This Euler step is only first order accurate but will be improved upon later. The time step restrictions for the numerical stability of (25) are particularly severe, especially in the case of turbulent flows so the next fractional step is designed to stabilize the scheme.

(iv) Viscous stabilization

$$\bar{\bar{u}} - \left(\frac{\sigma}{|F'|^2} \Delta t\right) \nabla^2 \bar{\bar{u}} = \bar{u} - \left(\frac{\sigma \Delta t \nu}{|F'|^2}\right) \nabla^2 u_n \tag{26}$$

with

$$\bar{\bar{u}} = 0 \qquad @ \qquad \eta = 0$$

Here σ is an optimising parameter for stability and accuracy. The stabilization step is implemented along the lines of the poisson algorithm (i.e. via eigen function expansions)

(v) Local extrapolation

For time dependant problems requiring accurate time transients, a local extrapolation procedure (10) is used to achieve global second-order accuracy in time.

II. B METHOD OF SOLUTION FOR CODE II

The basic algorithm for Code II contains the five fractional steps discussed above. There are qualitative differences in Code I and II; these differences arise because the boundary conditions at $X = 0, 2\pi$ are different. Because Tchebycheff polynomials are used in X direction also, the equation (24) for poisson equation for Code II is of the form

$$\sum_{m=0}^{Nc} \sum_{n=0}^{N2c} (\kappa_m + \lambda_n) P_{mn} = F_{mn} \qquad (27)$$

where κ_m are the eigen values in X direction and λ_n are the eigen values in Y direction; P_{ij}, F_{ij} are the decomposed modal components of p(X,Y) and f(X,Y) in the eigen space (m, n).

In the next section results are reported from these codes using,

(i) up to 32 Fourier modes and 64 Tchebycheff modes for Code I.

(ii) 16 Tchebycheff and 32 Tchebycheff modes for Code II. Typically the computer codes run at 2 ms per retained mode per time step on CDC 6600 computer.

III. LAMINAR TEST RESULTS

A large number of laminar flows over wavy walls were done using Codes I & II. Results from three representative runs will be described here.

Run 1 - The flow situation here is over a very gentle wave (wave surface $y = a\cos(kx)$ where $a = 2.54\ \mu$, $k = 1.2566\ mm^{-1}$, $ka = 3.19 \times 10^{-3}$) at a Reynolds number $Re_x = 4 \times 10^5$ with a starting length at entrance $X = 0.287m$, so the boundary layer thickness is 0.3 cm. This experiment is appropriate for comparison with Kelvin-Helmholz theory and Benjamin's theory (which requires $ka \ll 1$, $Re_x \gg 1$). For this flow, the Kelvin-Helmholz inviscid analysis predicts $C_p = 2ka = 6.3 \times 10^{-3}$. The pressure distribution predicted for this flow by this theory is 180° out of phase with the wall. On the other hand, Benjamin's theory predicts a phase shift of 217° and $C_p = 1.8 \times 10^{-4}$. The results obtained using Code I indicates excellent agreement with Benjamin's theory. The phase of the pressure distribution was found to be 214° ± 5° behind the surface displacement and the pressure coefficient was found to be $C_p = 1.742 \times 10^{-4}$ at the wall. In Fig. 2, the contours of pressure at steady state are plotted. The rate of decay of the pressure distribution away from the wall in this calculation is not in agreement with the predictions of Benjamin's theory. Close to the wall the pressure decays very slowly; at $ky = .78$ the pressure has decayed only by a factor 0.8238, so $p \sim \frac{1}{y}$, whereas the theory predicts decay of the pressure $p \sim e^{-ky}$. At intermediate distances away from the wall, the computer

calculations show that the pressure decay returns to e^{-ky} gradually. In Fig. 3, contours of velocity in the y direction are plotted. It is apparent from the figures that the y - velocity distribution peaks at a small distance from the wall and has phase lag of 63° with the surface.

Run 2. - The second run is similar to the first run except that the amplitude of the surface displacement is increased to $ka = 5.5 \times 10^{-2}$. Kelvin-Helmholz' theory predicts Cp = 0.11 for this case indicating that the wave amplitude is much too large to be analysable through pure inviscid theory. The Benjamin' theory predicts a phase shift of 217° with $Cp = 3.34 \times 10^{-3}$. Computer calculations indicate pressure coefficient $Cp = 3.3 \times 10^{-3}$ and a phase lag of 215 ± 6°. Again the rate of pressure decay near the wall disagrees with theoretical models.

Run 3. - The third run involves similation of experiments by Kachanov et. al.[11] Here $k = 25mm^{-1}$ while $ka = (5.3 \pm .01) \times 10^{-2}$. The Reynolds number for the flow is $Rex = 1.1 \times 10^{5}$. $U_{\infty} = 5.3$ m/sec. The boundary layer thickness at the start of the computational domain is .6 cm where X = 3.06 cm. In Fig. 4, the contours of the x-component of the velocity are plotted at a steady state. From Fig. 4, it is seen that there is a thickening and thinning of the boundary layer in the trough and crest regions of the wave. In Fig. 5, contours of the y-velocity are plotted; as before, the maxima and minima lag in phase by about 63°. In Fig. 6, contours of the pressure in the unmapped x-y domain are plotted from the

figure, the maximum pressure is found to be considerably smaller than the minimum pressure so the disturbance due to the wall is no longer linearizable; in fact, $p_{min} = 5.2 \times 10^{-3}$ while $p_{max} = 4.5 \times 10^{-3}$. Comparison of the fluctuation amplitude Δu at the height of unperturbed boundary layer thickness between the experiment and our calculations indicates excellent agreement.

IV. NON SYMMETRIC WAVES

The flow over nonsymmetrical periodic waves can also be computed using the present code. Here we report on calculations for two such nonsymmetrical waves. The wall amplitude and wavelength are the same as that in the Kachanov et al[11] experiment. Also, the flow conditions are kept the same as in the latter experiment in order to see whether the flow over nonsymmetrical waves can be beneficial for drag reduction. In Fig. 7 the grid lines are shown for one such nonsymmetrical wave. The conformal nature of the transformation is not apparent in this grid plot because the x, y length scales are different. In Fig. 8, contours of the x - velocity are plotted. As before, we see a thickening and thinning of the boundary layer thickness corresponding to decreasing and increasing wall skin friction. The noisy contour near the high is due to the sensitivity of the contour to small discretization errors. In Fig. 9, contours of the y-velocity are plotted. There is a marked change in the phase shifts of the peaks and valleys of the velocity relative to the wave surface. In Fig. 10, pressure contours are plotted. The magnitude of C_p is about the same as in Kachanov et al experiment. However, the pressure distribution has a maximum almost 180° ahead of the wave peak and a minimum about 80° ahead of the trough. Obviously, the skin friction and pressure distributions for this flow are quite different from those of the symmetrical wave surface. Nevertheless, there

are only small changes in both the integrated friction drag and pressure drag from the Kachanov et al experiment, which we estimate has a net drag reduction of about 5% compared to a flat plate.

In Fig. 11, the grid system for the second nonsymmetric wave is plotted. Again, the flow conditions as well as the wall amplitude and wavelength are the same as in the Kachanov et al experiment. In Fig. 12, contours of the x-velocity distribution at a steady state are plotted. The thickening and thinning of the boundary layer profiles is again apparent. In Fig. 13, the y-velocity is contoured. It is apparent that the highs and lows of the y-velocity are markedly different in both magnitude and location. Because of the long duration of favorable pressure gradient, the activity is quite low (small negative y-velocity) in the cusp regions. The steep rise of adverse pressure gradient causes increased activity on the lee-side of the wave.

In Fig. 14, the pressure distribution for this wave is presented. Again, the amplitude and phase of the pressure distribution is markedly changed. However, the integrated frictional drag and pressure drag show no significant change from the Kachanov et al, experiment.

Flow over Bumps

In Fig. 15, 16, 17 the flow calculations over a finite bump are reported. The bump is Gaussian and Fig. 15 shows the computational grid system. In Fig. 16, the pressure contours are plotted. Fig. 17 shows the x-velocity distribution over the bump

V. FUTURE DIRECTION FOR WORK

APPLICATIONS OF THE NAVIER-STOKES CODES TO OTHER PROBLEMS

The computer algorithms developed in this report have been used to study turbulent flow over wavy walls. The experiments chosen to study have been that of Kendall[1] and Sigal[2]. Currently, the effects of turbulence are solved outside the code itself via a boundary layer program which uses multi-equation turbulence modelling. The mechanics of such analysis are described below.

(i) The boundary layer program requires the self generated pressure distribution which is obtained from the Navier Stokes Code.

(ii) The Navier Stokes Code uses the lumped eddy stresses from the boundary layer program. Fig. 18 shows the pressure distribution obtained by the Navier Stokes Code using this technique over a Kendall surface. The experimental value of pressure coefficient for this problem is Cp = 0.1; our calculations show a pressure coefficient of Cp = 0.13. The phase of the pressure distribution obtained by our analysis compares extremely well with the experiment of Kendall. The disagreement in the amplitude of the pressure distribution indicates that, turbulence modelling be done directly within the Navier Stokes Code itself rather than through the boundary layer program. Basically a time transient code such as ours changes the mean flow profiles with time and hence the turbulent stresses have to change accordingly. The interaction

technique described above is inadequate to handle this situation.

One of the chief dilemmas concerning incorporation of turbulence modelling in a Navier Stokes Code such as this revolves around the inadequate experimental data over which such models may be compared with.

The inflow-outflow code (Code II) will be an excellent start off point for such investigations. Unfortunately, contractural constraints of finite time objectives often leave such work in jeopardy.

The inflow-outflow code can also be used to analyse convected eddies within the computational domains. Presently such investigations are being conducted at LaRC. Due to the extreme sensitivity of the code to smooth initial data, such experiments can not be reported at the present time.

This work was supported by NASA Langley Research Center under contract NAS1-15754.

REFERENCES

1. Kendall, J. M., "Laminar Boundary Layer on a Wavy Wall", J. Fluid Mech., Vol. 41, 1970, pp. 259-281.

2. Sigal, A., Ph. D. Thesis, California Institute of Technology, 1971.

3. Lamb, H., Hydrodynamics, 6th Edition, Cambridge University Press, Chapter IX, 1932.

4. Miles, J. W., "On the Generation of Surface Waves by Shear Flows", J. Fluid Mech., Vol. 3, 1957, pp. 185-204.

5. Benjamin, T. B., "Shearing Flows Over a Wavy Boundary", J. Fluid Mech., Vol. 6, 1959, pp. 161-205.

6. Davis, R. E., "On the Prediction fo Turbulent Flow Over a Wavy Boundary", J.Fluid Mech., Vol. 42, 1970, pp. 721-731.

7. Zilker, D. P., Jr., Ph. D. Thesis, University of Illinois, 1976.

8. Markatos, N. C. G., "Heat, Mass, and Momentum Transfer Across a Wavy Boundary", Computer Methods in Appl. Mech. and Eng., Vol. 14, 1978, pp. 323-376.

9. Meiron, D. I., Orszag, S. A., and Israeli, M., "Applications of Numerical Conformal Mapping", Cambridge Hydrodynamics Report No. 34, 1980.

10. Deville, M. and Orszag, S. A., "Splitting Methods for Incompressible Flow Problems", Cambridge Hydrodynamics Report No. 32, 1980.

11. Kachanov, Yu. S., Kozlov, V. V., Kotjolkin, Yu. D., Levchenko, V. Ya., and Rudnitsky, A. L., Acta Astronautica, Vol. 2, 1975, pp. 557-559.

FIGURE TITLES

Figure 1. Plot of Mapped grid system used in computation. The wave surface is a sine wave (Ka = 0.1963). The orthonomality of grid lines is apparent in this plot.

Figure 2. Contours of pressure at a steady state for Run I ($ka = 3.19 \times 10^{-3}$, flow is laminar at $Re_x = 4 \times 10^5$).

Figure 3. Contour of y-velocity distribution for Run I.

Figure 4. Contours of x-velocity at a steady state for the experiment of Kachanov et al". (Run III).

Figure 5. Contour of Y-velocity for Run III.

Figure 6. Contours of pressure for Run III.

Figure 7. Computational grid system for nonsymmetric wave (Laminar flow $Re_x = 1.1 \times 10^5$).

Figure 8. Contours of x-velocity over nonsymmetric wave.

Figure 9. Contours of y-velocity over a nonsymmetric wave.

Figure 10. Contours of pressure for flow over nonsymmetric wave.

Figure 11. Grid system for the second nonsymmetric wave (Laminar flow, $Re_x = 1.1 \times 10^5$).

Figure 12. Contours of x-velocity at steady state for the second nonsymmetric wave.

Figure 13. Contours of y-velocity at steady state for the second nonsymmetric wave.

Figure 14. Contours of pressure at a steady state for the second nonsymmetric wave.

Figure 15. Computational grid system for flow over a periodic gaussian bump. (Laminar flow $Re_x = 1.1 \times 10^5$)

Figure 16. Contours of pressure at steady state for flow over a periodic bump.

Figure 17. Contours of x-velocity for flow over a periodic bump.

Figure 18. Contours of pressure at steady state for turbulent flow over wavy surface corresponding to the experiment of Kendall.[1]

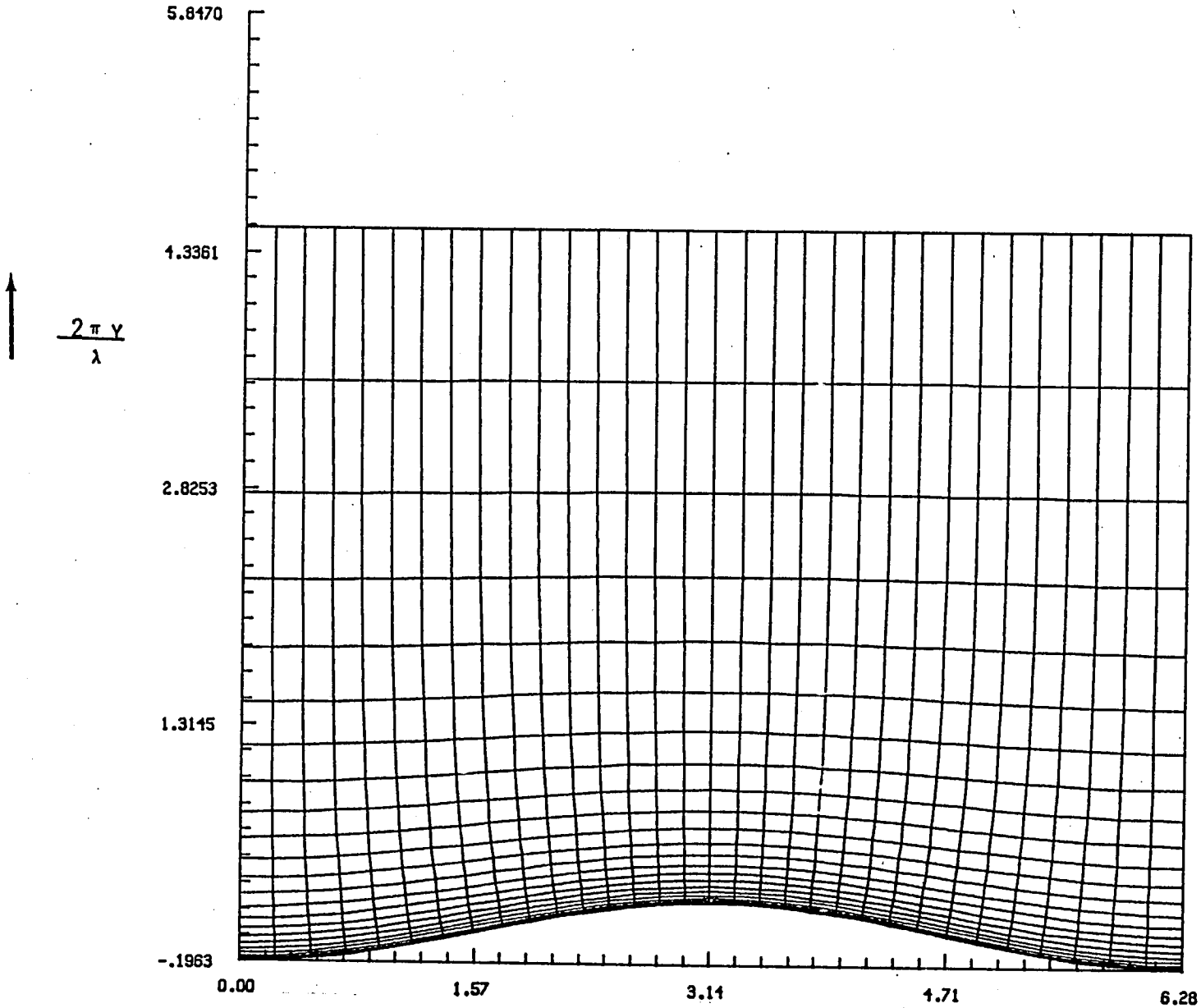

Figure 1. Plot of Mapped grid system used in computation. The wave surface is a sine wave (Ka = 0.1963). The orthonomality of grid lines is apparent in

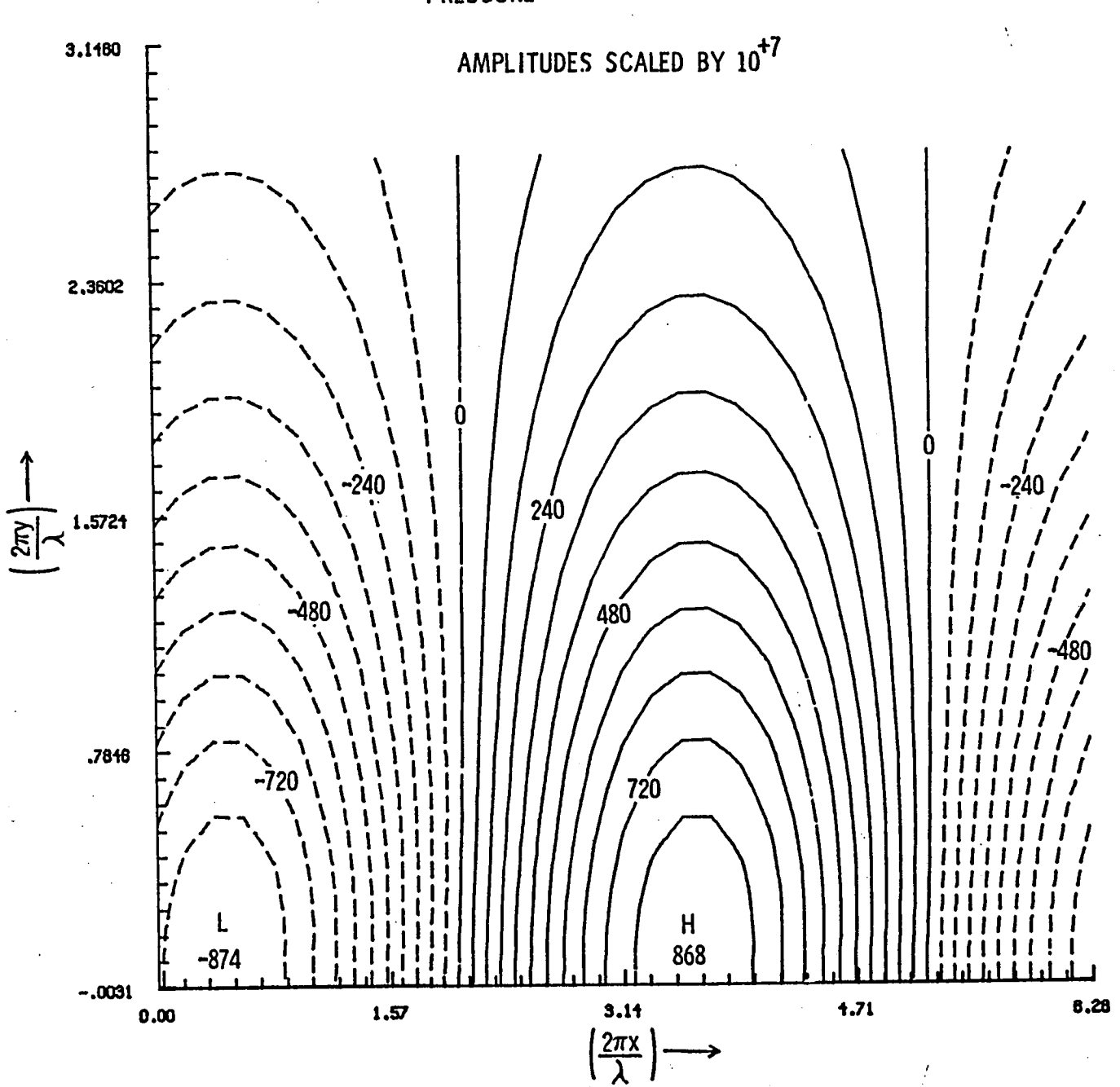

Figure 2. Contours of pressure at a steady state for Run I ($ka = 3.19 \times 10^{-3}$, flow is laminar at $Re_v = 4 \times 10^5$).

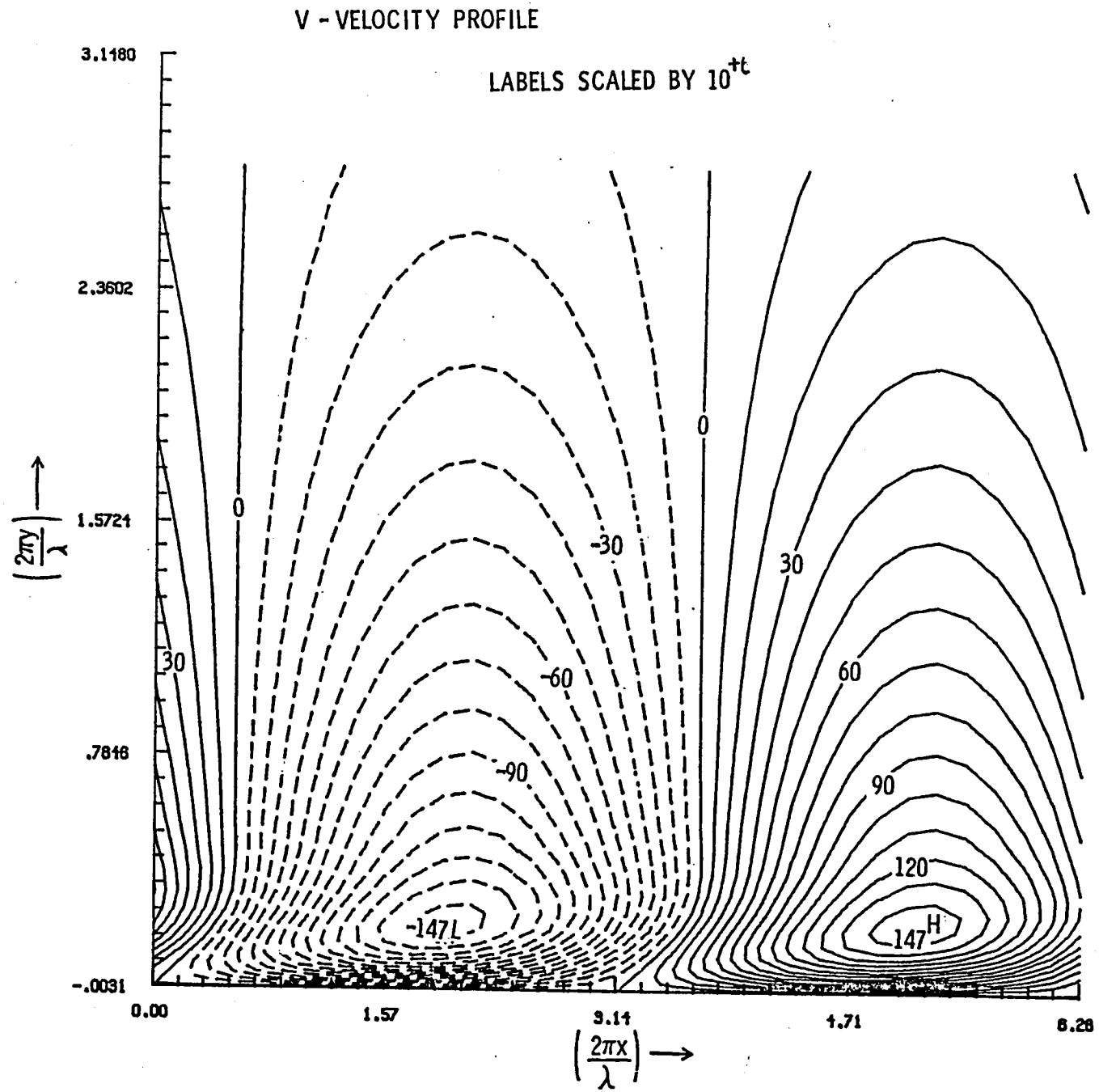

Figure 3. Contour of y-velocity distribution for Run I.

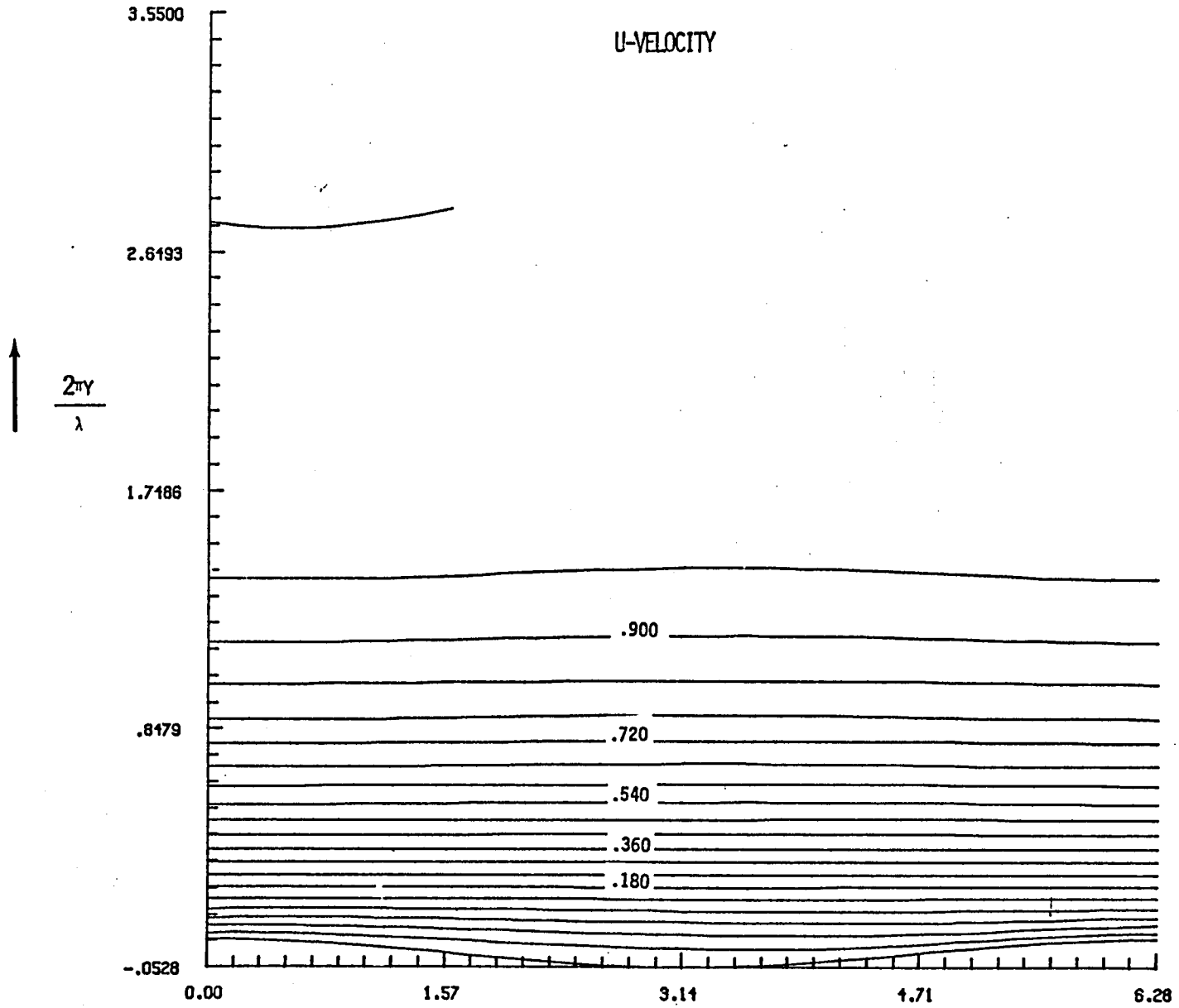

Figure 4. Contours of x-velocity at a steady state for the experiment of Kachanov et al". (Run III).

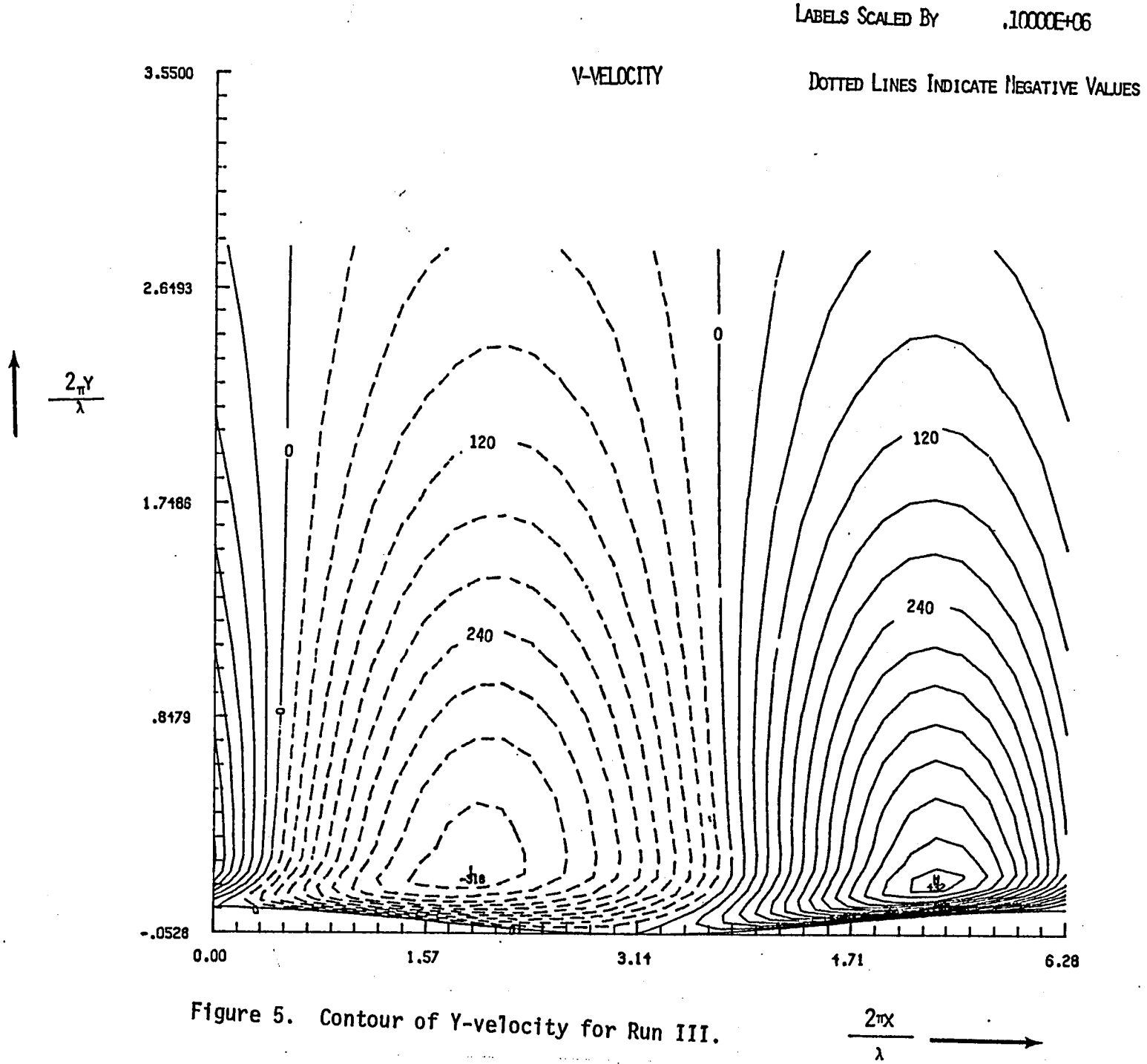

Figure 5. Contour of Y-velocity for Run III.

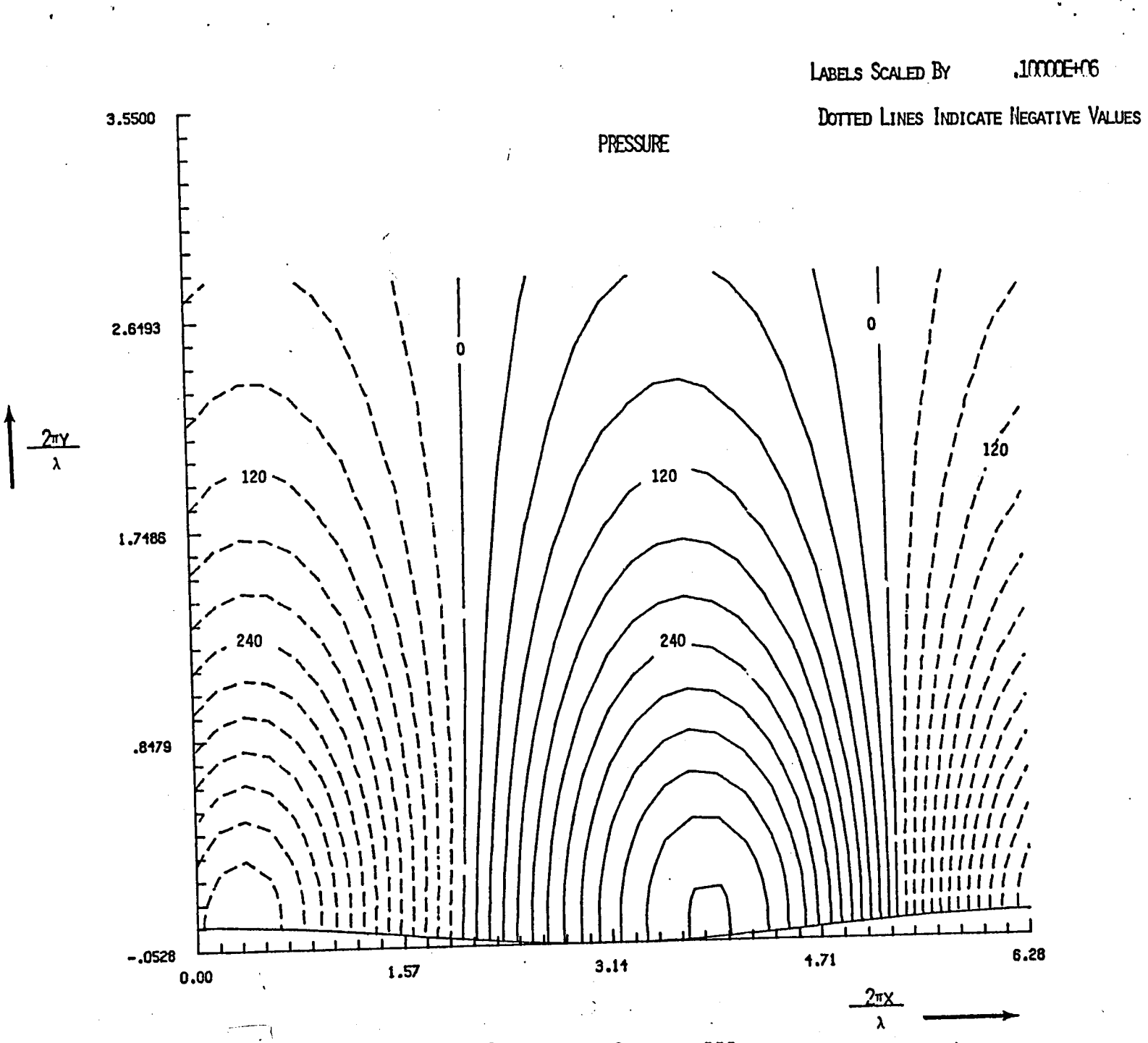

Figure 6. Contours of pressure for Run III.

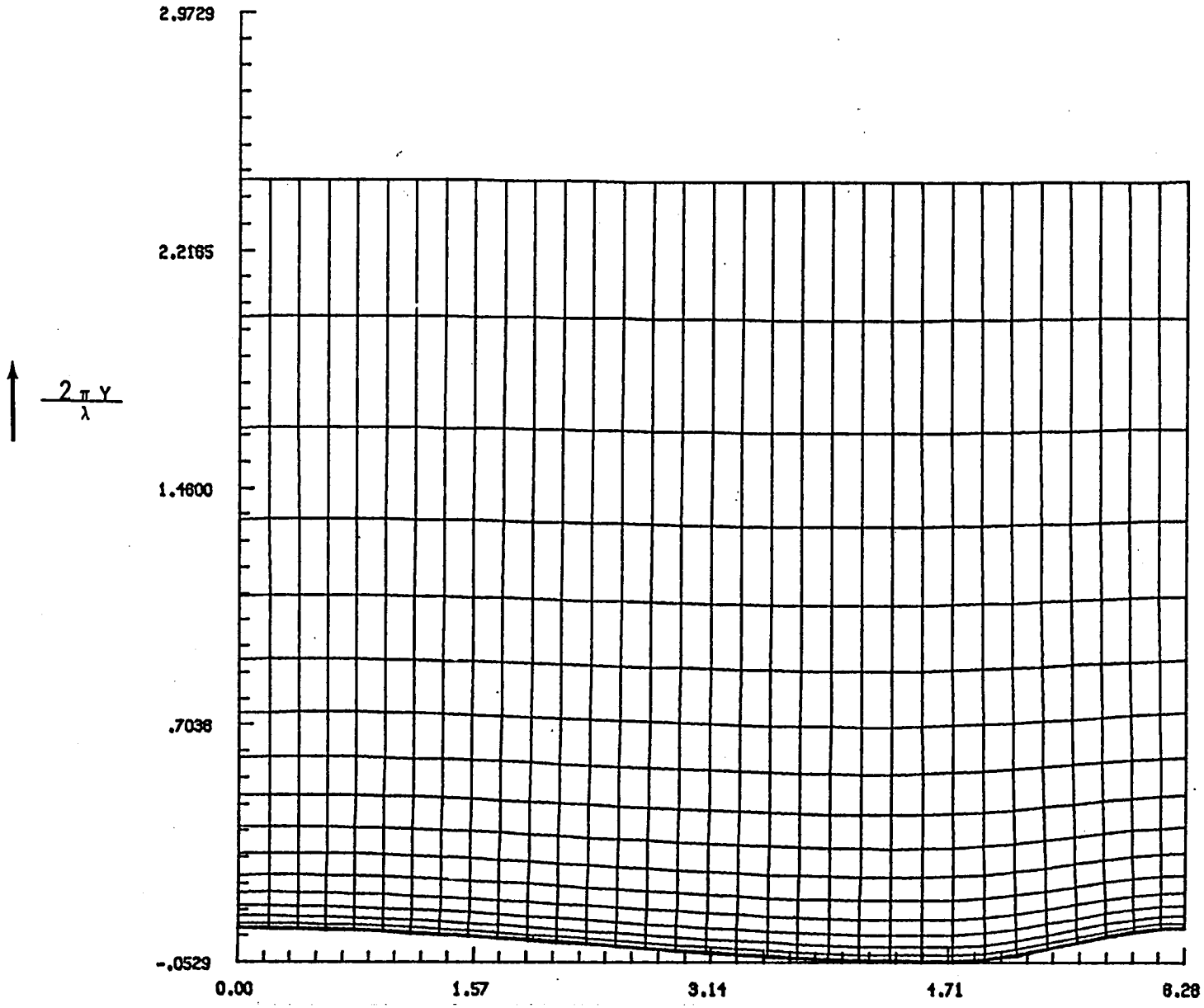

Figure 7. Computational grid system for nonsymmetric wave (Laminar flow $Re_\chi = 1.1 \times 10^5$).

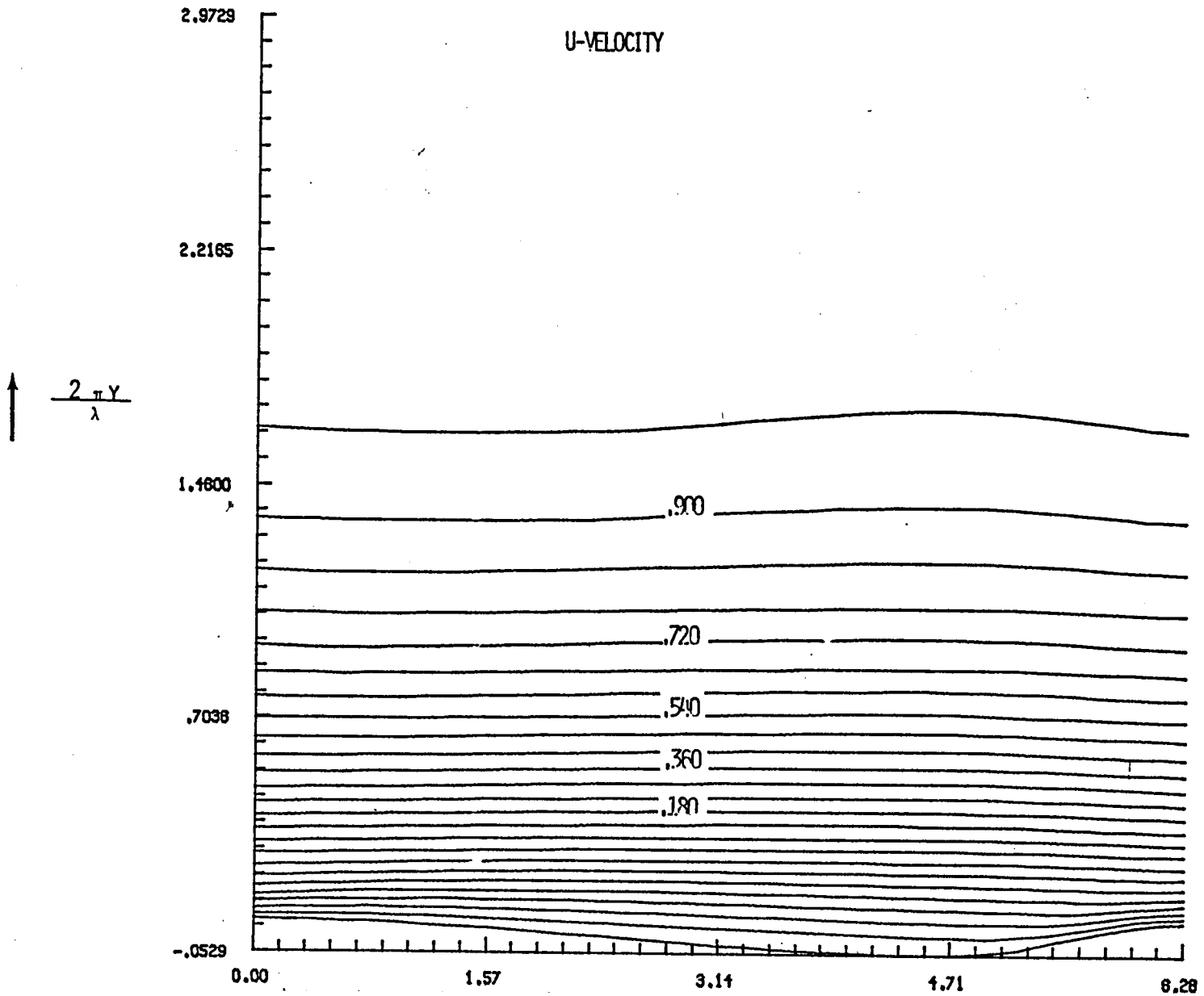

Figure 8. Contours of x-velocity over nonsymmetric wave.

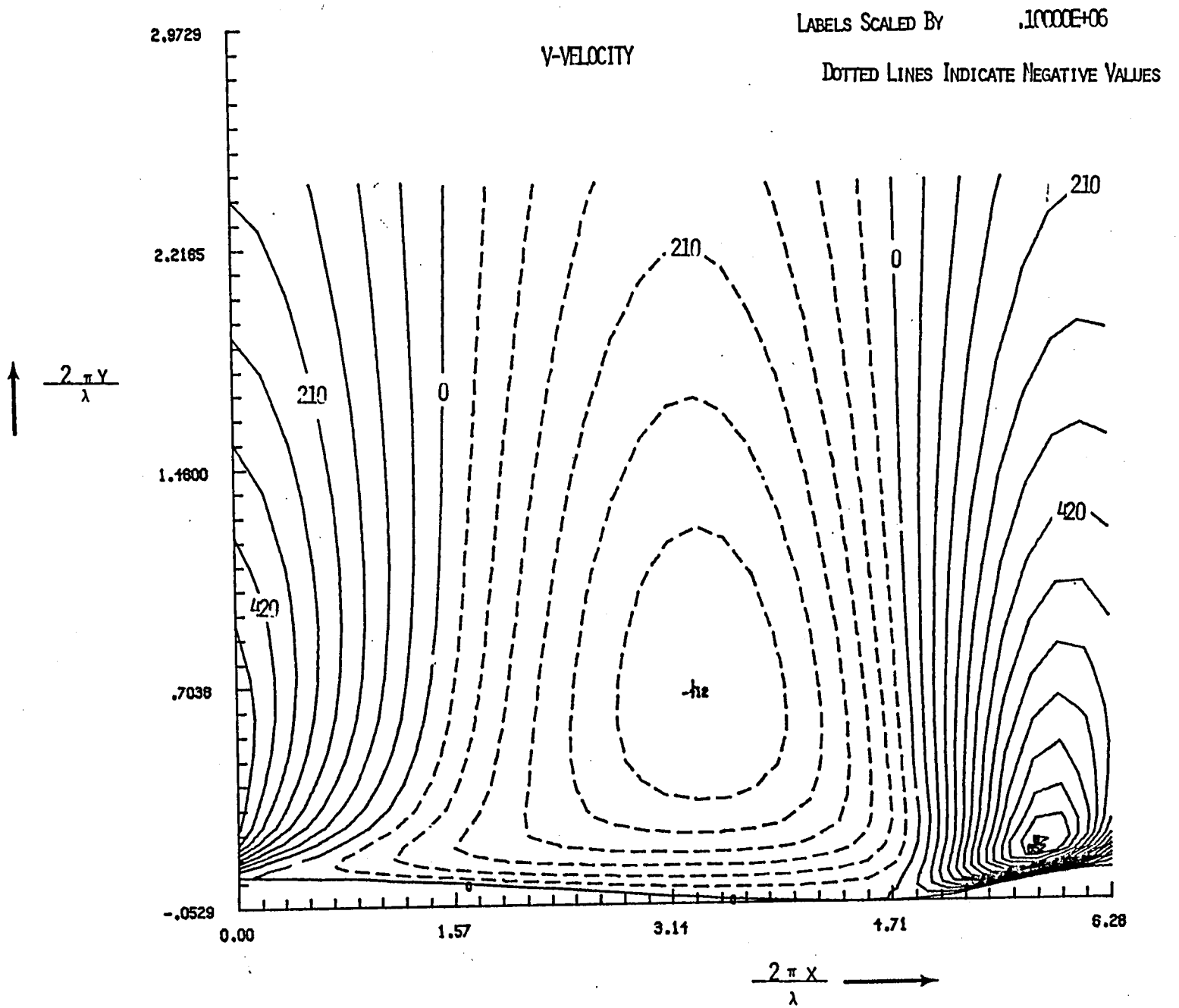

Figure 9. Contours of y-velocity over a nonsymmetric wave.

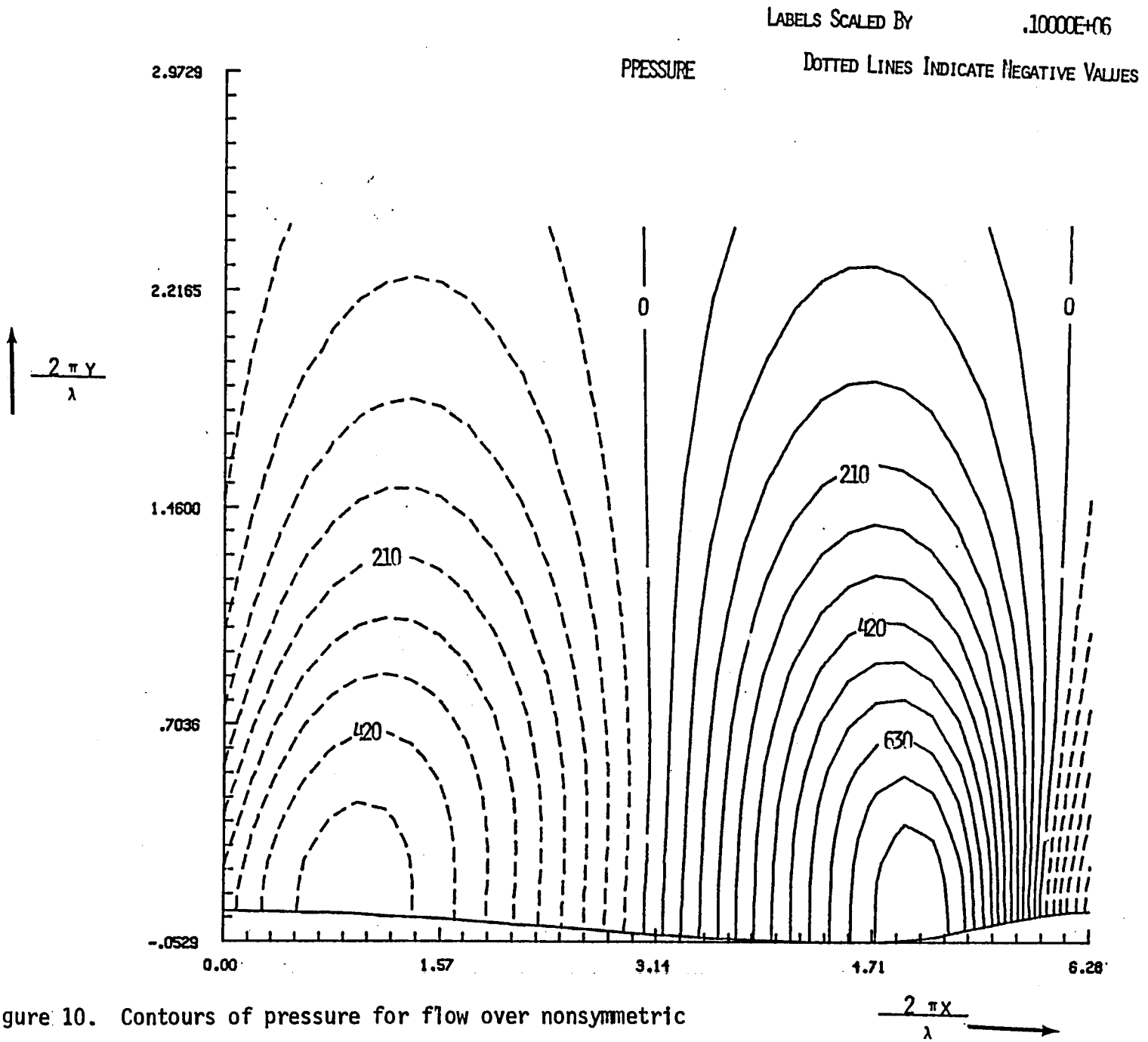

Figure 10. Contours of pressure for flow over nonsymmetric wave.

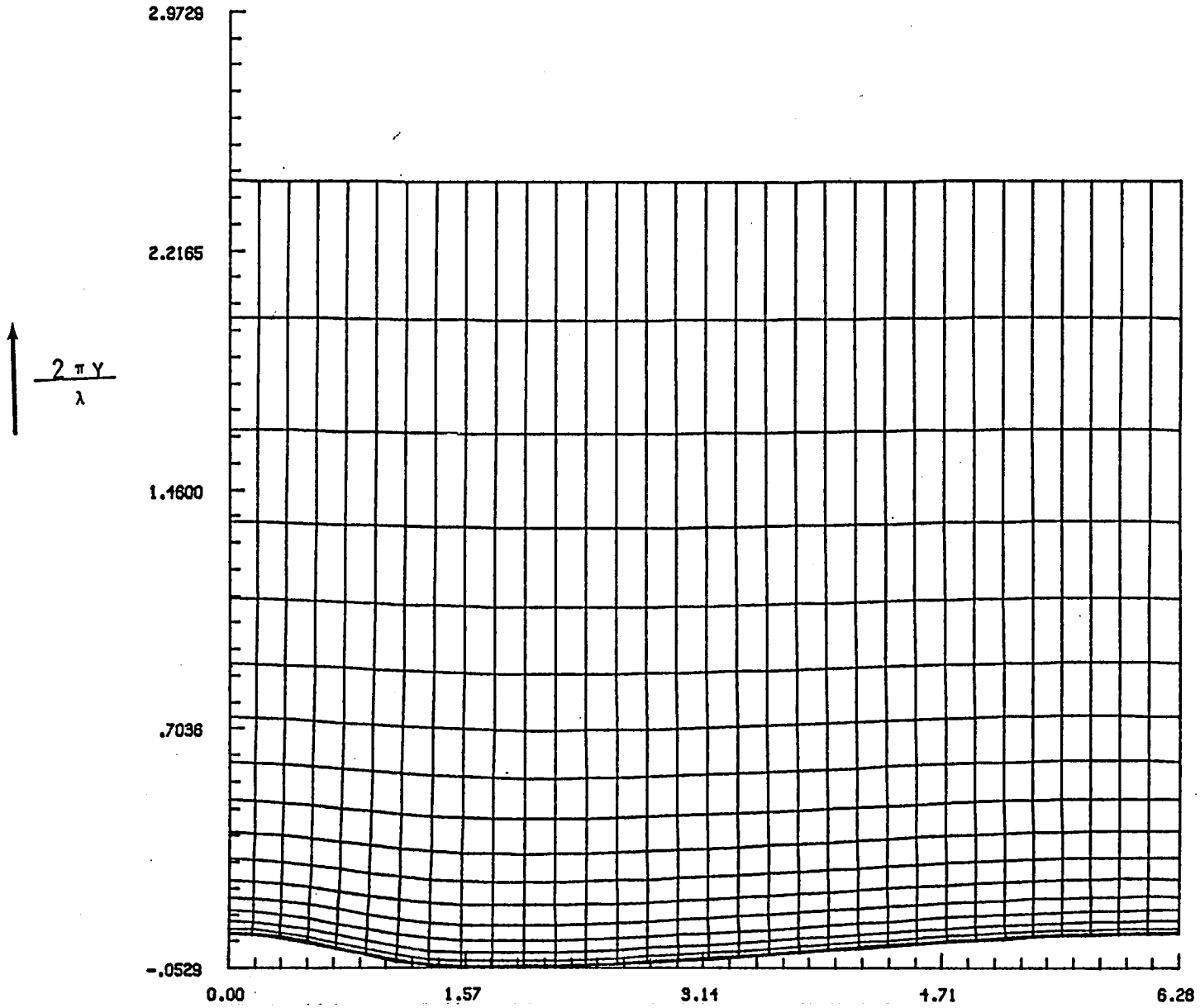

Figure 11. Grid system for the second nonsymmetric wave (Laminar flow, $Re_\chi = 1.1 \times 10^5$).

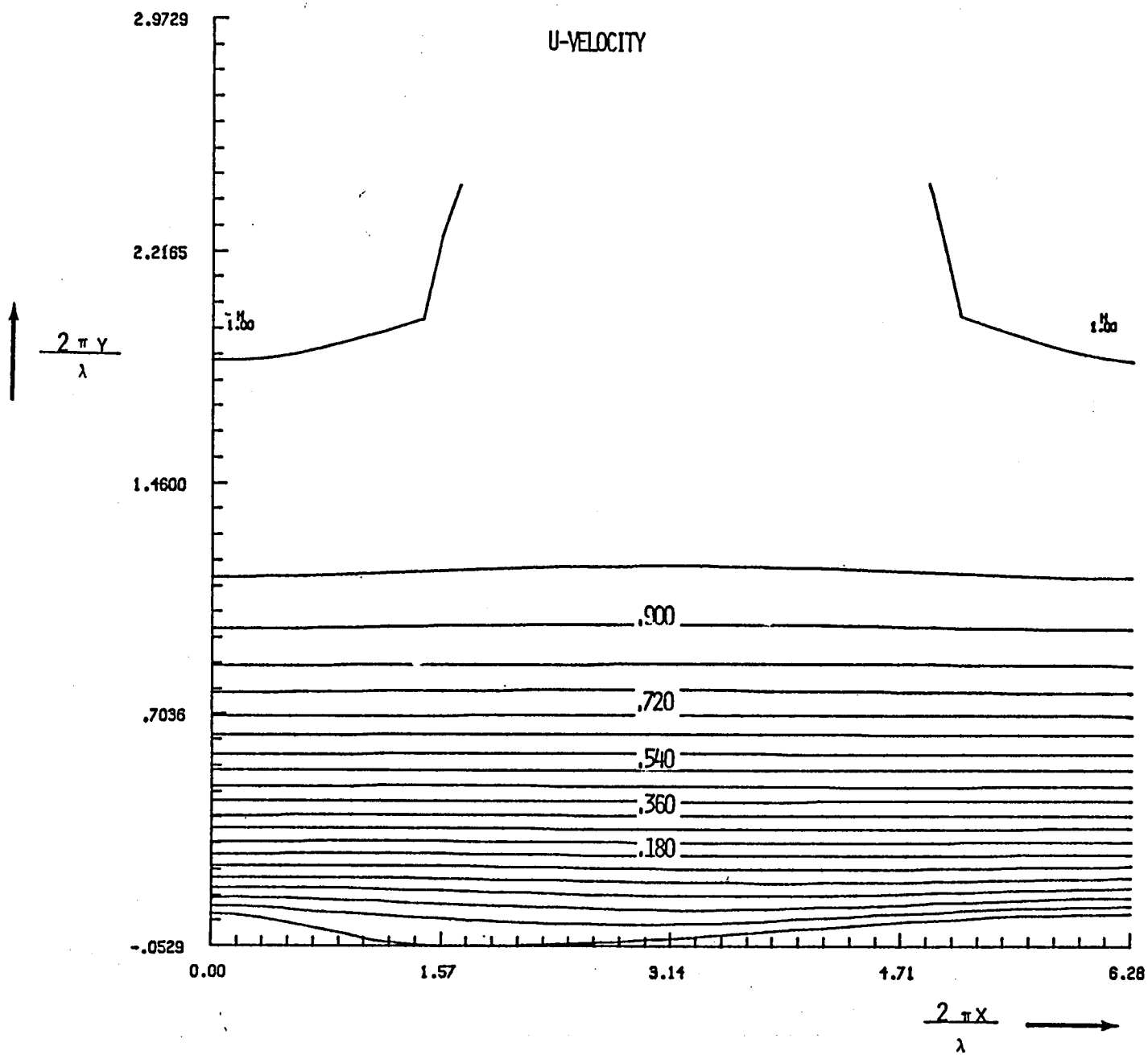

Figure 12. Contours of x-velocity at steady state for the second nonsymmetric wave.

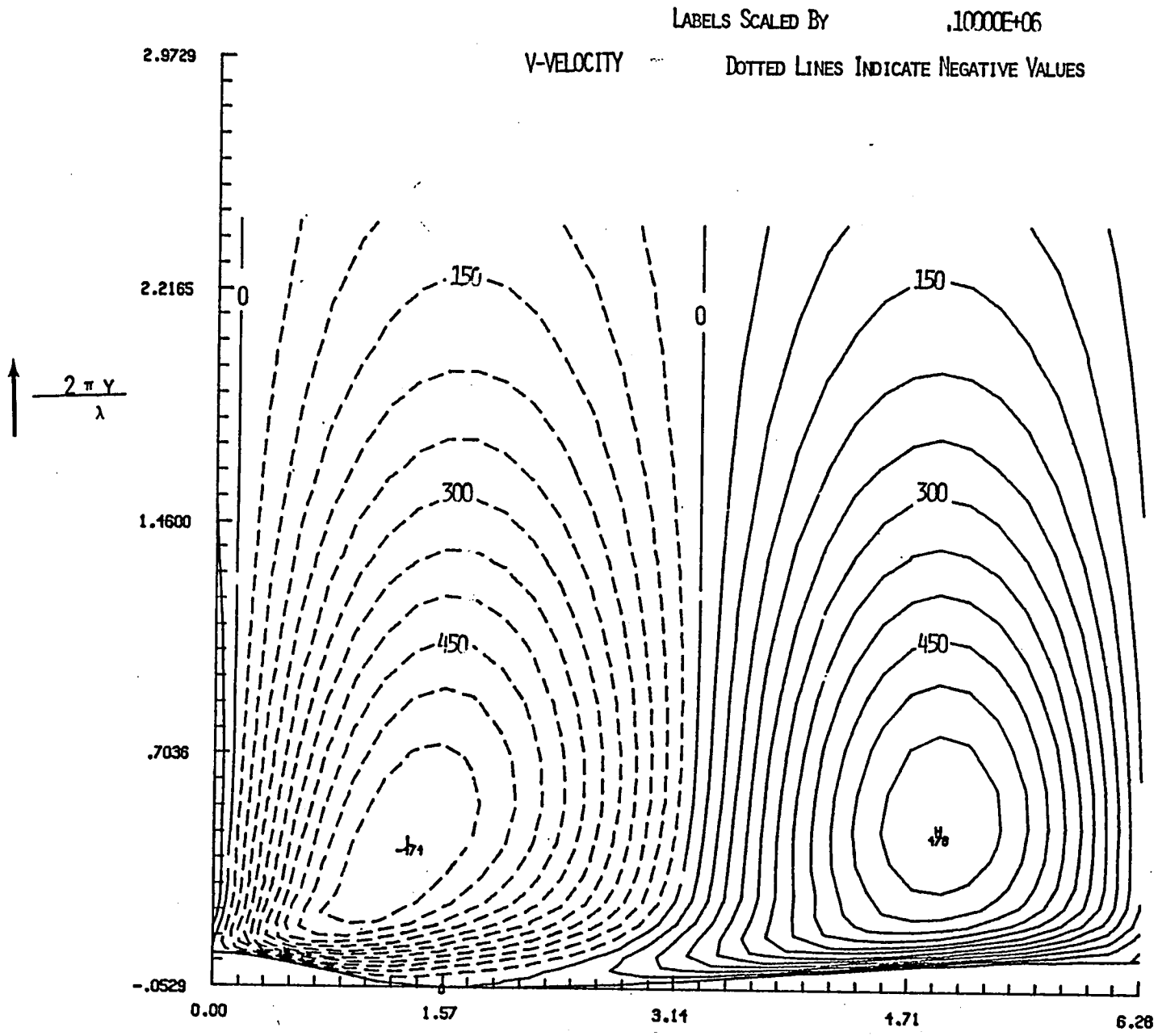

Figure 13. Contours of y-velocity at steady state for the second nonsymmetric wave.

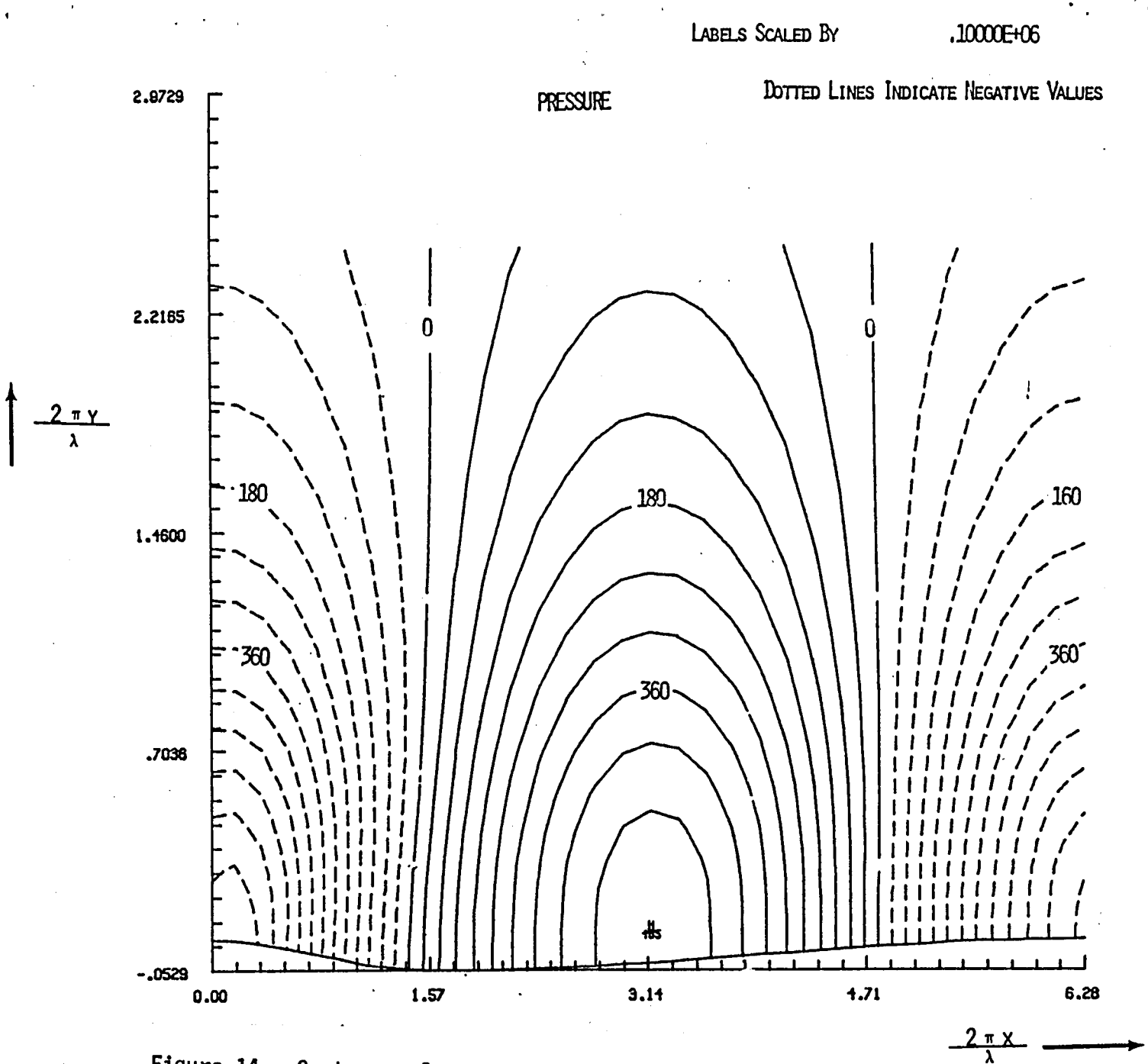

Figure 14. Contours of pressure at a steady state for the second nonsymmetric wave.

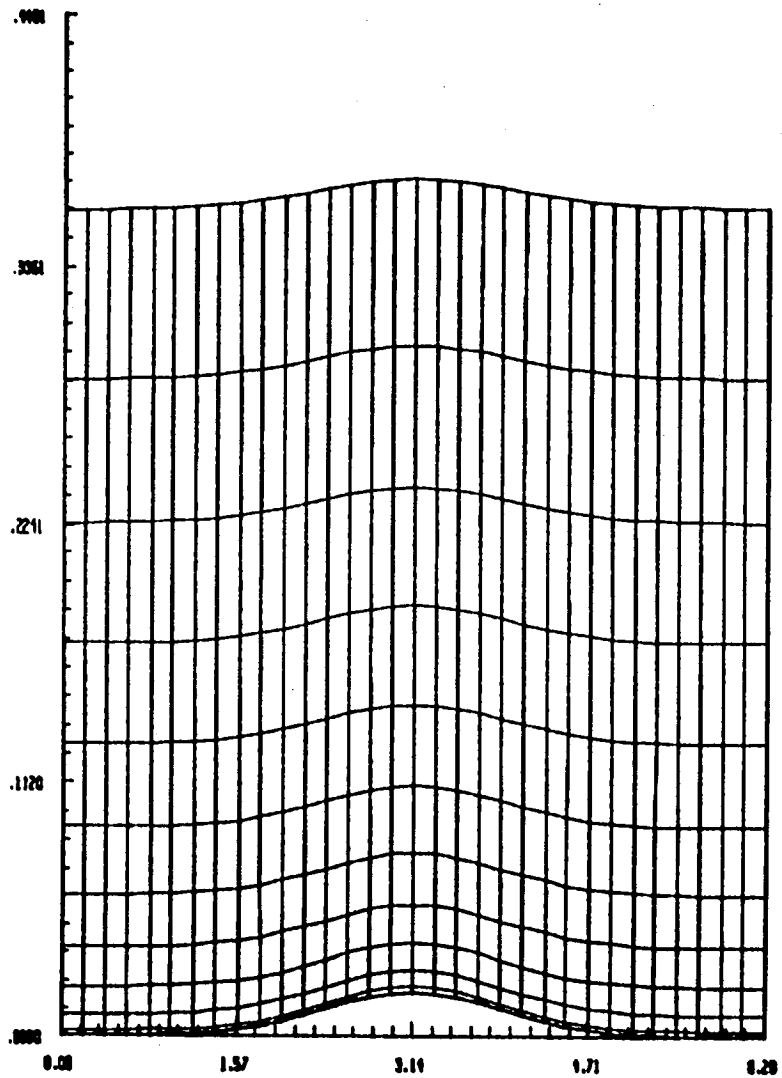

Figure 15. Computational grid system for flow over a periodic gaussian bump. (Laminar flow $Re_X = 1.1 \times 10^5$)

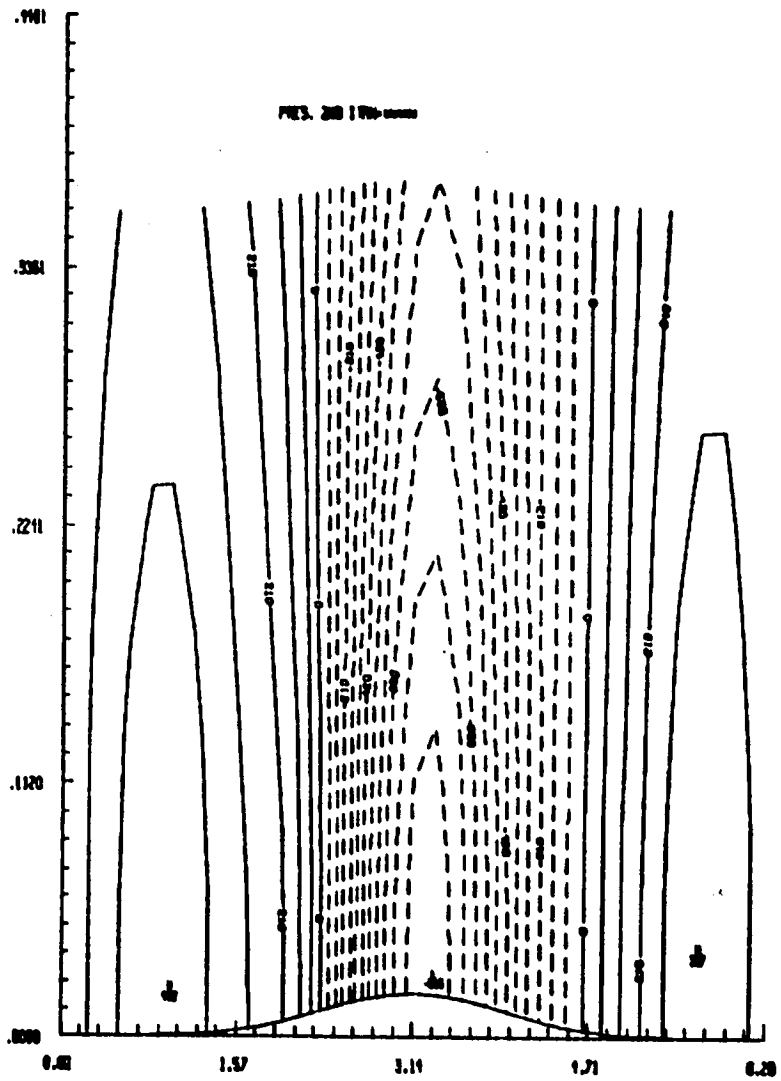

Figure 16. Contours of pressure at steady state for flow over a periodic bump.

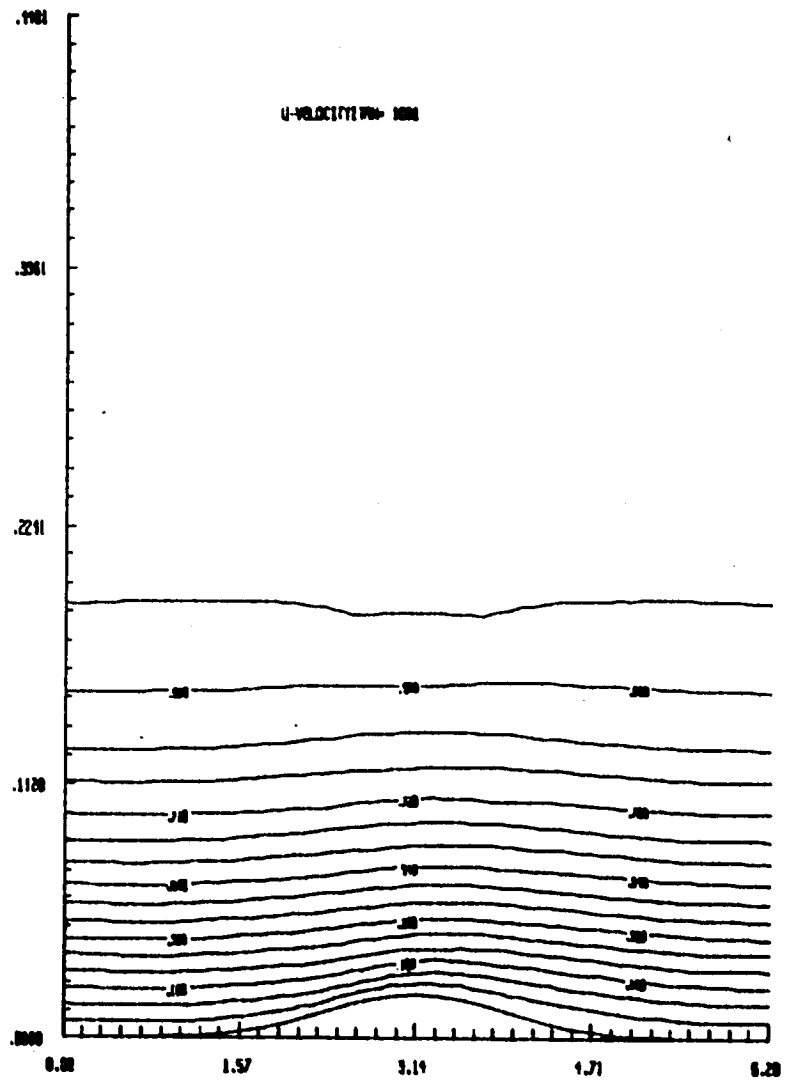

Figure 17. Contours of x-velocity for flow over a periodic bump.

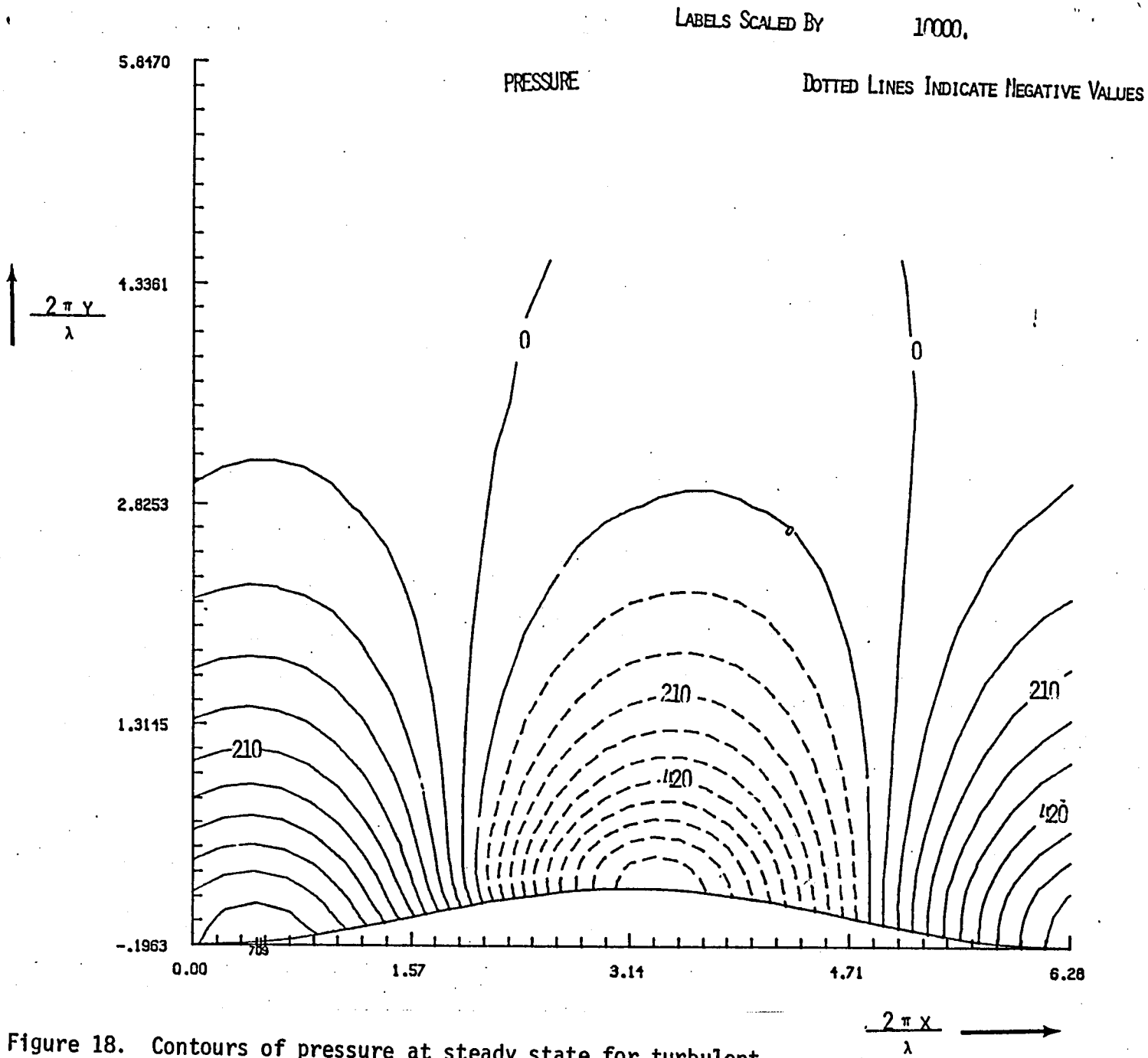

Figure 18. Contours of pressure at steady state for turbulent flow over wavy surface corresponding to the experiment of Kendall.(1)

End of Document